Nanographene Oxide–Hyaluronic Acid Conjugate for Photothermal Ablation Therapy of Skin Cancer

Ho Sang Jung,[†] Won Ho Kong,[†] Dong Kyung Sung,[‡] Min-Young Lee,[†] Song Eun Beack,[†] Do Hee Keum,[†] Ki Su Kim,[§] Seok Hyun Yun,[§] and Sei Kwang Hahn[†,§,*]

[†]Department of Materials Science and Engineering, Pohang University of Science and Technology (POSTECH), San 31, Hyoja-dong, Nam-gu, Pohang, Kyungbuk 790-784, Korea, [‡]Department of Pediatrics, Samsung Medical Center, Sungkyunkwan University, School of Medicine, Seoul 135-710, Korea, and [§]Wellman Center for Photomedicine, Department of Dermatology, Harvard Medical School and Massachusetts General Hospital, 65 Landsdowne Street UP-5, Cambridge, Massachusetts 02139, United States

ABSTRACT Melanoma skin cancer is one of the most dangerous skin cancers and the main cause of skin-cancer-related mortality. Hyaluronic acid (HA) has been used as an effective transdermal delivery carrier of chemical drugs and biopharmaceuticals. In this work, a nanographene oxide–HA conjugate (NGO–HA) was synthesized for photothermal ablation therapy of melanoma skin cancer using a near-infrared (NIR) laser. Confocal microscopy and *ex vivo* bioimaging clearly visualized the remarkable transdermal delivery of NGO–HA to tumor tissues in the skin of mice, which might be ascribed to highly expressed HA receptors and relatively leaky structures around tumor tissues, enabling the enhanced permeation and retention of nanoparticles. The NIR irradiation resulted in complete ablation of tumor tissues with no recurrence of tumorigenesis. The antitumor effect was confirmed by ELISA for caspase-3 activity and histological and immunohistochemical analyses with TUNEL assay for tumor apoptosis. Taken together, we could confirm the feasibility of transdermal NGO–HA for photothermal ablation therapy of melanoma skin cancers.

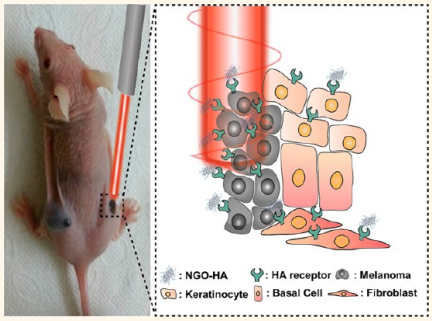

KEYWORDS: nanographene oxide · hyaluronic acid · photothermal therapy · skin cancer

Nanosized graphene oxide (NGO) has been widely investigated for biomedical applications due to its unique physical, mechanical, and optical properties.[1,2] In particular, NGO and reduced NGO have a high photothermal effect under low-power near-infrared (NIR) irradiation due to their effective light-to-heat conversion compared to other carbon allotropes.[3] Although *in vitro* photothermal ablation of cancer cells has been successfully performed using the NGO systems,[4,5] *in vivo* photothermal therapy has been limited likely due to the safety issues of NGO.[6] To alleviate the safety issues and improve the stability of NGO, NGO was conjugated to poly(ethylene glycol) [NGO-PEG], which was accumulated in tumor tissues of mice by the enhanced permeation and retention (EPR) effect after systemic delivery. The NIR irradiation on the tumor site resulted in the effective ablation of tumor cells.[7] The biodistribution of iodine-125-labeled NGO-PEG revealed that NGO-PEG was mainly accumulated in the reticuloendothelial system (RES) and gradually excreted *via* renal and fecal pathways.[8] The *in vivo* biodistribution study has shown the possibility of NGO derivatives for further biomedical applications.

Hyaluronic acid (HA) has been regarded as one of the best biopolymers in terms of safety issues and widely used for various biomedical applications including drug delivery[9,10] and tissue engineering.[11] Recently, we reported the transdermal delivery of the HA–human growth hormone (hGH) conjugate by HA receptor-mediated delivery through the skin tissues of epidermis and dermis after hydration of stratum corneum by the hygroscopic HA.[12] Fluorescence microscopy clearly visualized the penetration of the FITC-labeled HA–hGH conjugate through the dorsal skin of mice. The structural hydrophobic domain of HA can facilitate its penetration into skin tissues.[13,14] Especially, tumor cells are known to have overexpressed HA receptors like cluster

* Address correspondence to skhanb@postech.ac.kr.

Received for review July 15, 2013 and accepted December 30, 2013.

Published online January 02, 2014
10.1021/nn405383a

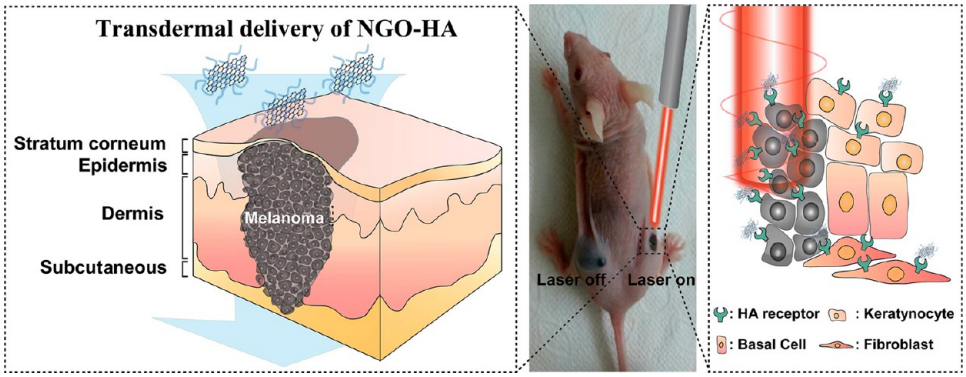

Figure 1. Schematic illustration for the transdermal delivery of nanographene oxide–hyaluronic acid (NGO–HA) conjugates into melanoma skin cancer cells and the following photothermal ablation therapy using a near-infrared (NIR) laser.

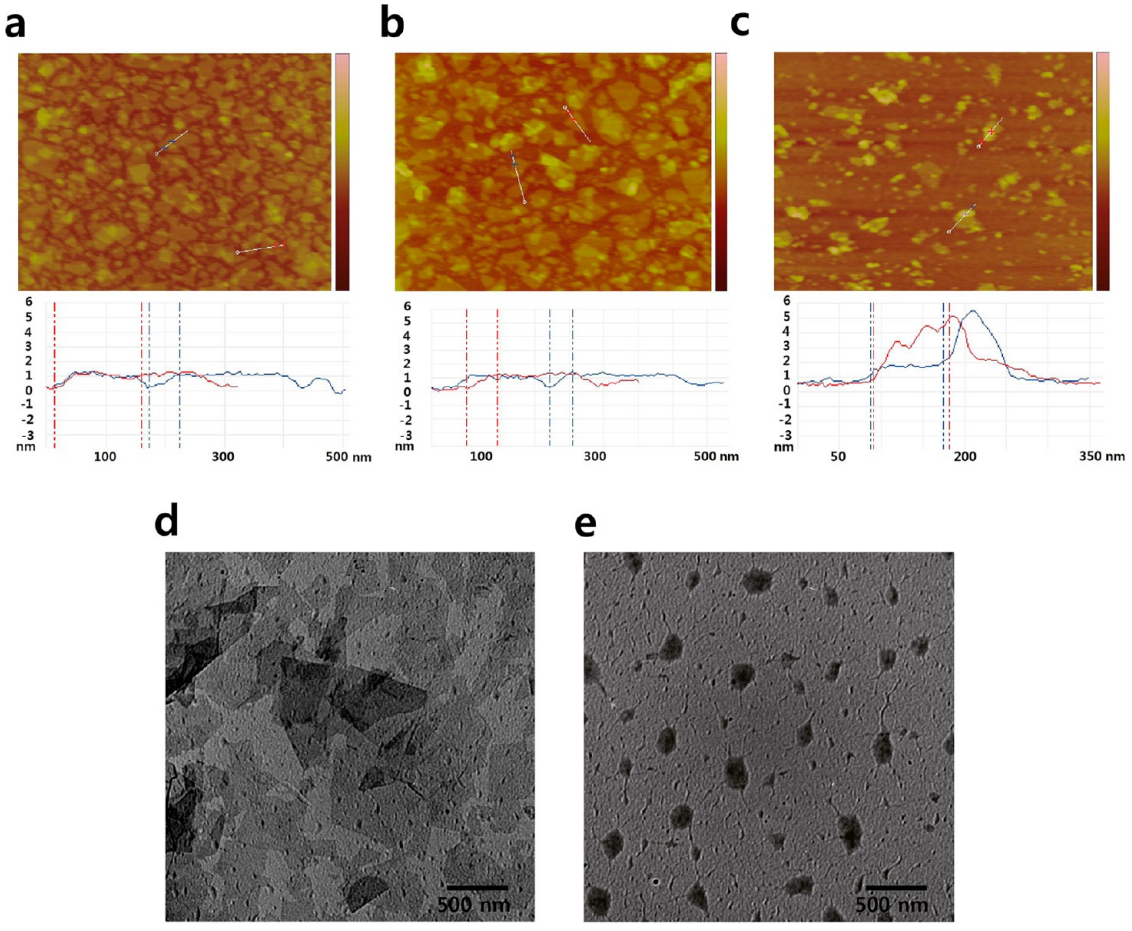

Figure 2. Atomic force microscopic (AFM) images of (a) nanographene oxide (NGO), (b) NGO–COOH, and (c) NGO–hyaluronic acid (HA). TEM images of (d) GO and (e) NGO–HA.

determinant 44 (CD44)[15] and lymphatic vessel endothelial HA receptor-1 (LYVE-1)[16] on the cell surface. Tumor cells are susceptible to heat treatment, resulting in cell death above 43 °C.[17] A variety of hyperthermal treatment methods have been proposed for the treatment of cancers using gold nanoparticles,[18] iron oxide nanoparticles,[19] and carbon nanomaterials.[20]

Here, we report transdermal NGO–HA conjugates for photothermal ablation therapy of melanoma skin cancer using a NIR laser as schematically shown in Figure 1. Melanoma is less common, but it is one of the most dangerous skin cancers infiltrating deeply into the skin. It is known to be the main cause of skin-cancer-related death.[21] To our knowledge, this is the first report to deliver NGO through a transdermal pathway and treat skin cancer with NIR irradiation. The NGO–HA was thought to be transdermally delivered to tumor tissues in the skin of mice with highly expressed HA receptors and relatively leaky structures rendering the enhanced permeation and retention of

nanoparticles. This system might be safer than systemic delivery systems because NGO is directly and locally accumulated in tumor tissues by the transdermal pathway, minimizing the possible side effect of NGO in the body. After bioimaging for the transdermal delivery of NGO–HA labeled with NIR fluorescent Hilyte647, we demonstrated and discussed the photothermal ablation therapy of NGO–HA for melanoma skin cancer in mice.

RESULTS AND DISCUSSION

Preparation and Characterization of NGO–HA. Carboxylated NGO (NGO–COOH) was prepared by the tip sonication and the activation of microsized GO solution with chloroacetic acid in a strong basic condition. Then, hexamethylene diamine (HMDA)–HA was synthesized[22] and conjugated to NGO–COOH for the preparation of NGO–HA by amide bond formation using the EDC chemistry. The successful synthesis of NGO–HA was confirmed by atomic force microscopy (AFM), transmission electron microscopy (TEM), Fourier transform infrared spectroscopy (FT-IR), and Raman spectroscopic analyses. As shown in AFM images, NGO had a lateral size of *ca.* 200 nm and a thickness of *ca.* 1.04 nm (Figure 2a). NGO–COOH showed no significant increase in thickness (Figure 2b). After conjugation with HA, the thickness increased to 4–5 nm, while the lateral size was not changed (Figure 2c). TEM revealed a spherical morphology of NGO–HA with a mean particle size of *ca.* 250 nm due to the wrapping and folding of NGO by HA (Figure 2d,e). According to FT-IR analysis (Supporting Information Figure S1), we could observe the characteristic amide bond (–CO–NH–) stretching vibration at 1650 cm^{-1}, the methyl group on *N*-acetyl-D-glucosamine (one of HA repeating unit) at 2900 cm^{-1}, and the increased peak of ether (–C–O–C–) on HA near 1100 cm^{-1} after conjugation of HA to NGO–COOH. Raman spectroscopy of NGO and NGO–HA showed the characteristic D band (~1350 cm^{-1}) and G band (~1580 cm^{-1}) peaks (Figure S2). The increased D/G ratio indicated the thermal reduction of uncarboxylated oxides in NGO during the carboxylation. All of these results confirmed the successful functionalization of HA onto NGO. Then, the physiological stability of NGO, NGO–COOH, and NGO–HA was examined in deionized (DI) water and 100 mM NaCl solution. All of NGO, NGO–COOH, and NGO–HA were soluble and remained stable in water. However, NGO and NGO–COOH were aggregated and precipitated in 100 mM NaCl solution. NGO–HA remained stable in the NaCl solution as well as water without aggregation for several months, reflecting the physiological stability for further *in vivo* applications (Figure S3).

***In Vitro* Photothermal Ablation of NGO–HA.** To assess the light-to-heat conversion capability of NGO–HA, the solution temperature increase by irradiation of the NIR laser (808 nm, 2 W/cm^2) for 10 min was recorded at various NGO–HA concentrations (Figure 3a). At a concentration of NGO–HA above 250 μg/mL, NIR irradiation for 10 min increased the temperature of NGO–HA solution around 40 °C, which was considered to be high enough for photothermal ablation of cancer cells. Then, the cytocompatibility of NGO–HA was assessed in B16F1 melanoma and Detroit 551 human skin fibroblast cells by MTT assay at various concentrations of NGO–HA. After incubation for 24 h, the cytotoxicity of NGO–HA appeared to be negligible up to the concentration of 200 μg/mL in both cells, but the cytotoxicity was slightly higher in melanoma cells than fibroblast cells (Figure 3b). Then, the photoablation

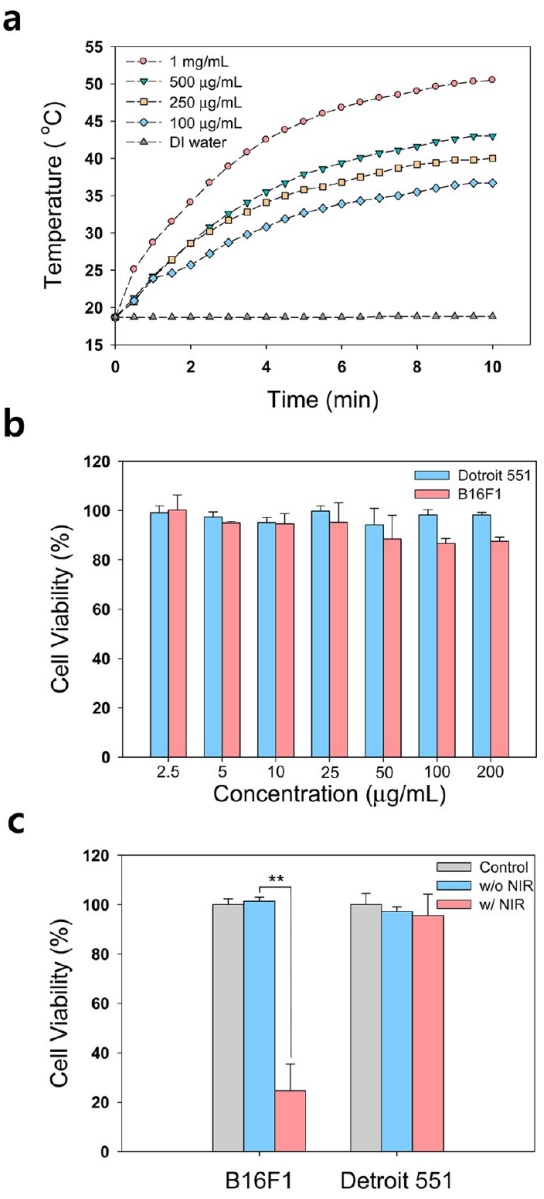

Figure 3. (a) Photothermal effect of nanographene oxide–hyaluronic acid (NGO–HA) conjugates at various concentrations. (b) Cytocompatibility of NGO–HA in B16F1 melanoma and Detroit 551 fibroblast cells with increasing concentration. (c) Effect of photothermal ablation of NGO–HA on the viability of B16F1 melanoma and Detroit 551 cells ($P < 0.001$).**

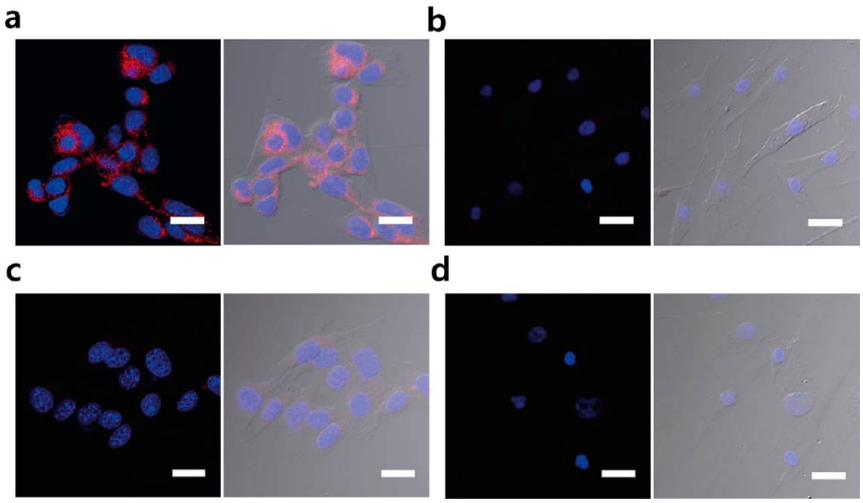

Figure 4. ***In vitro*** **confocal microscopic analysis of nanographene oxide–hyaluronic acid (NGO–HA) conjugates up-taken to (a,c) B16F1 cells (scale bars = 30 μm) and (b,d) Detroit 551 cells (scale bars = 50 μm) (a,b) without and (c,d) with HA preincubation.**

of NGO–HA was assessed in B16F1 melanoma and Detroit 551 cells with NIR irradiation. The NGO–HA treatment resulted in more effective photothermal ablation of cancer cells than normal skin cells (Figure 3c), which might be related with the uptake of NGO–HA to cancer cells *via* HA-receptor-mediated endocytosis.[23] The lack of heat defense system in cancer cells can cause more significant photoablation of cancer cells than normal cells by NGO–HA.[24] In contrast, more than 96% of fibroblast cells survived after irradiation of near-infrared light (Figure 3c), reflecting the cytocompatibility of the NGO–HA treatment.

HA-Receptor-Mediated Targeting of NGO–HA to Cancer Cells. After incubation of melanoma and fibroblast cells with Hilyte647 dye-labeled NGO–HA, *in vitro* confocal microscopic analysis was carried out to compare the cellular uptake of NGO–HA. Both B16F1 and Detroit 551 cells are known to express HA receptors on their surfaces.[25,26] At the same condition, much stronger intensity of NGO–HA–Hilyte647 was observed inside cancer cells than normal cells (Figure 4a,b). The competitive binding tests in the presence of free HA (Figure 4c,d) confirmed the receptor-mediated endocytosis of NGO–HA into cancer cells.

Transdermal Delivery of NGO–HA into Normal and Cancerous Skin. On the basis of the successful transdermal delivery of HA–hGH conjugates,[12] we carefully investigated the transdermal delivery of NGO–HA through the normal (Figure S4) and cancerous skin (Figure 5) in comparison with NGO–PEG. Confocal laser scanning microscopy revealed that the transdermally delivered NGO–HA–Hilyte647 remained embedded on the top of the normal skin even after vigorous washing (Figure S4c, left). The NGO–HA with a particle size of *ca.* 250 nm might not be easy to deeply penetrate the normal skin. In some regions, however, we could observe the fluorescent signal from the transdermally delivered NGO–HA–Hilyte647, probably with a relatively small particle size (Figure S4c, right). Then, we carried out confocal laser scanning microscopy and *ex vivo* bioimaging to visualize the transdermal delivery of NGO–HA–Hilyte647 to SKH-1 hairless mice inoculated with B16F1 melanoma cells (Figure 5). Due to the transdermal characteristics of HA derivatives, NGO–HA–Hilyte647 was significantly delivered through the damaged cancerous skin barrier (Figure 5d).[27] The tumor growth under the skin might form leaky structures around tumor cells and tissues and increase the skin permeation, rendering the effective transdermal delivery of NGO–HA into tumor tissues.[27] The red fluorescence of NGO–HA–Hilyte647 was observed in every tissue site including stratum corneum, epidermis, dermis, and tumor tissue. The fluorescence of NGO–HA–Hilyte647 could be detected from the top and even from the bottom of the dissected 5 mm long tumor tissues (Figure 5e). The deep penetration of NGO–HA into the tumor tissues can be explained by the diffusion of NGO–HA through the interstitial tumor space covering about 40% of the tumor volume.[28] Highly expressed HA receptors in tumor tissues might also facilitate the transdermal delivery of NGO–HA. In contrast, NGO–PEG–Lissamine was not delivered through both the normal skin (Figure S4b) and the cancerous skin (Figure 5c). After transdermal delivery, the remaining NGO–PEG on the skin was almost completely removed during the washing step. The nonfouling PEG might prevent the adhesion and the delivery of NGO–PEG to the skin. Considering all these results, we could confirm the effective transdermal delivery of NGO–HA to tumor tissues in the skin.

In Vivo **Photothermal Ablation Therapy of Skin Cancer.** The photothermal ablation therapy of skin cancer was carried out using NGO and NGO–HA in SKH-1 mice inoculated with B16F1 cells on both dorsal flanks. PBS

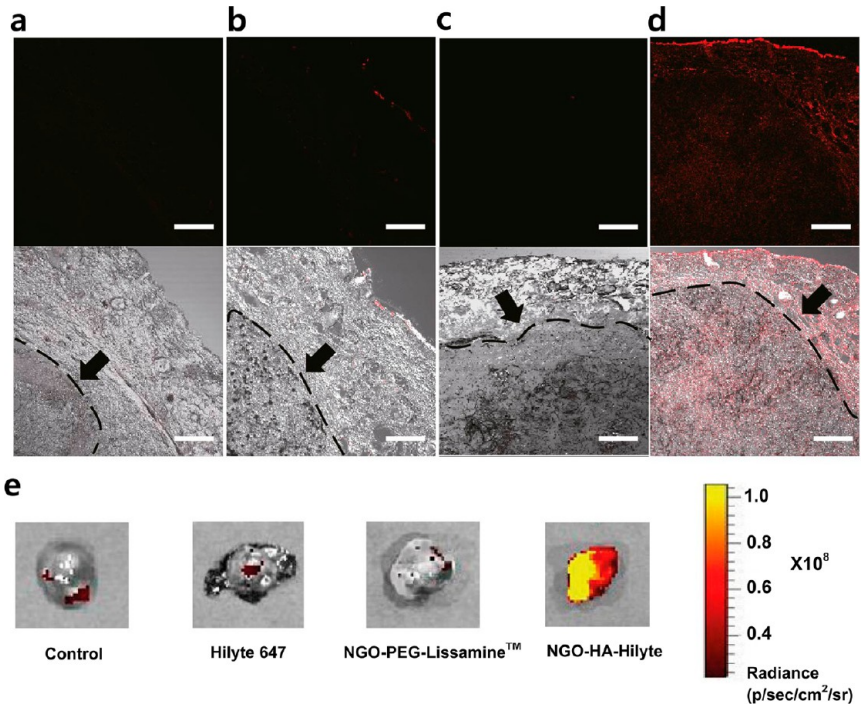

Figure 5. Confocal microscopic analysis for the transdermal delivery of (a) PBS, (b) Hilyte647 dye only, (c) nanographene oxide–poly(ethylene glycol)–Lissamine (NGO–PEG–Lissamine) and (d) NGO–hyaluronic acid–Hilyte647 (NGO–HA–Hilyte647) conjugates in tumor model mice (scale bar = 200 μm). Arrows indicate the tumor regions. (e) *Ex vivo* bioimaging of dissected tumor tissues.

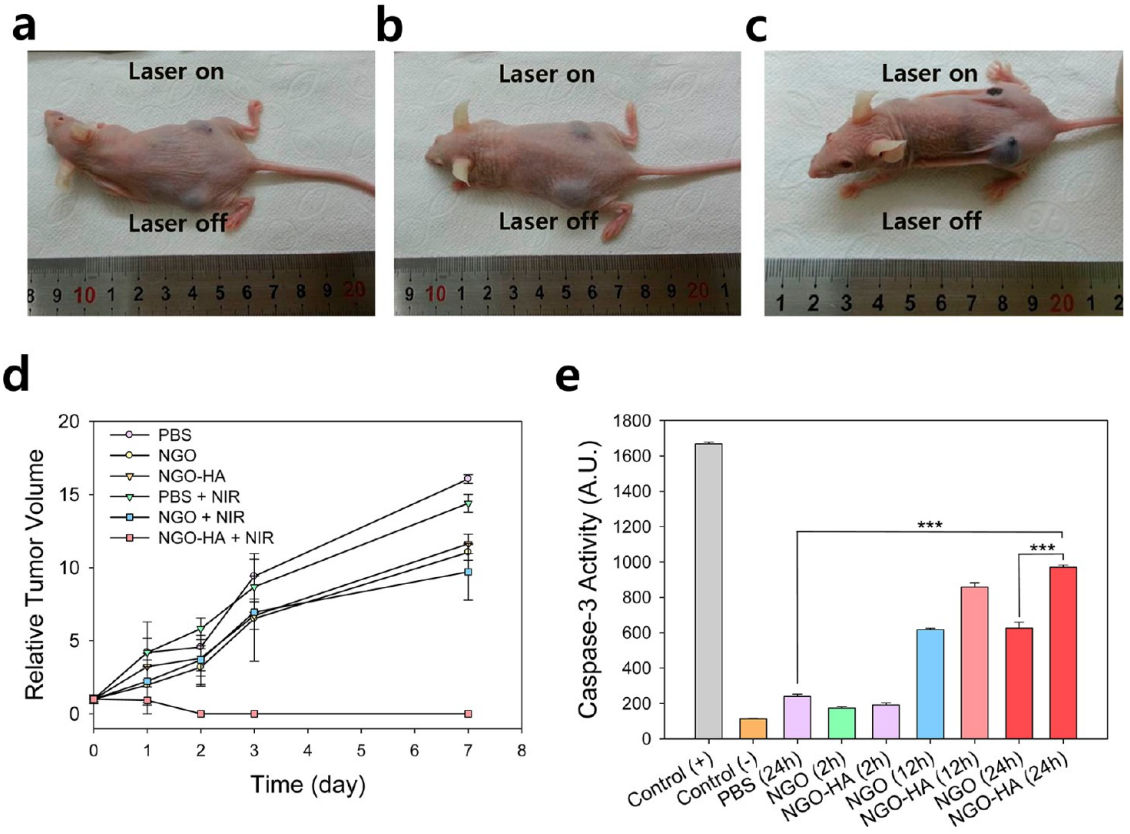

Figure 6. Photographs showing the effect of photothermal ablation therapy with NIR irradiation on the tumor growth in SKH-1 mice inoculated with B16F1 cells on both dorsal flanks after topical administration of (a) PBS, (b) nanographene oxide (NGO), and (c) NGO–hyaluronic acid (HA). (d) Relative tumor volume (V/V_0) with increasing time for a week. (e) Caspase-3 activity in tumor tissues by ELISA with increasing time for a day for the analysis of heat induced apoptosis (***$P < 0.0001$).

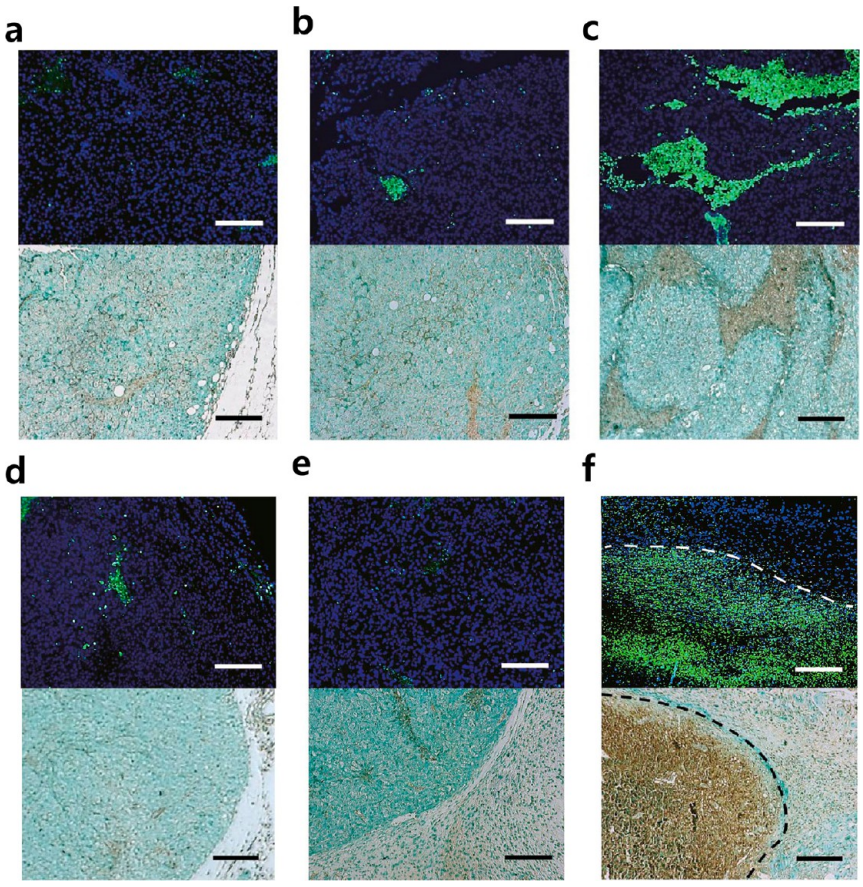

Figure 7. Histological TUNEL assay of tumor tissues after treatment with (a) PBS, (b) nanographene oxide (NGO), and (c) NGO–hyaluronic acid (HA) in the absence of NIR irradiation, and (d) PBS, (e) NGO, and (f) NGO–HA in the presence of NIR irradiation. Inside dotted lines indicate tumor regions (white scale bar = 200 μm and black scale bar = 100 μm).

as a control, 1 mg/mL of NGO and NGO–HA were topically administered on the skin of the tumor region for 30 min. One side of the dorsal flank was irradiated with NIR laser for 10 min, and the other side was not treated for comparison. The treatment with PBS and NGO showed no significant tumor ablation effect regardless of NIR irradiation (Figure 6a,b). In the case of NGO–HA, tumor tissues were not ablated without NIR irradiation but completely ablated by the photothermal therapy with NIR irradiation (Figures 6c and S5a). After photoablation of tumor tissues, there was no recurrence of tumorigenesis in comparison to continuous tumor growth for all the other treatment groups (Figure 6d). The remaining black wound after photoablation was recovered to the normal skin in a month (Figure S5b).

Histological Skin Cancer Apoptosis Analysis. The tumor tissues treated with PBS, NGO, and NGO–HA with and without NIR irradiation were harvested for the analysis of heat-induced apoptosis by the photothermal ablation therapy. After homogenization of each tissue, caspase-3, reflecting the apoptosis, was monitored by ELISA. Because there was no remaining tumor tissue after complete photoablation in 48 h, the caspase-3 activity was measured at 2, 12, and 24 h post-treatment. The caspase-3 activity after treatment with NGO–HA in the presence of NIR irradiation was statistically higher than that with PBS or NGO in 24 h (Figure 6e). The NIR irradiation enhanced caspase-3 activity for both cases of treatments with NGO and NGO–HA (Figure S6). The apoptosis degree of tumor cells treated with NGO–HA under NIR irradiation might increase further because the ELISA was performed in 1 day before the complete ablation of tumor tissues in 2 days.

Histological analysis for tumor apoptosis by the treatment with PBS, NGO, and NGO–HA in the absence and presence of NIR irradiation was carried out by fluorescence and immunohistochemical TUNEL assay. In the fluorescence TUNEL assay, the TUNEL-positive area was stained green and normal cell nuclei were stained blue. Immunohistochemical TUNEL assay stained the TUNEL-positive area brown and the normal region green. The treatment with PBS (Figure 7a,d) and NGO (Figure 7b,e) showed no significant TUNEL-positive area in the tumor region. After treatment with NGO–HA, the NIR irradiation resulted in more effective apoptosis of tumor cells than that without NIR irradiation, marking all the area inside the tumor TUNEL-positive (Figure 7c,f). All of

these results were consistent with those by ELISA, reflecting the feasibility of NGO−HA for the selective photothermal ablation therapy of melanoma skin cancer.

Furthermore, chemical drugs can be loaded to NGO in NGO−HA by $\pi-\pi$ stacking for transdermal chemo- and photothermal combination therapy of melanoma skin cancers. This technique has a great potential for clinical applications for treating skin cancer and other skin diseases. Many dermatologic problems, such as acne and non-melanoma skin cancers, tend to occur over a wide area in the face, for which focal needle-based delivery of therapeutic agents is not either clinically justifiable or effective. Local transdermal delivery is expected to cause much lower side effects by NGO in the body compared to systemic delivery. The application of NGO−HA may go beyond the photothermal therapy, transporting photosensitizers or other molecular drugs to target regions in the skin.

CONCLUSIONS

We successfully developed a transdermal NGO−HA conjugate for photothermal ablation therapy of melanoma skin cancer using a NIR laser. Confocal microscopy and *ex vivo* bioimaging clearly visualized the effective transdermal delivery of NGO−HA to tumor tissues. The NIR irradiation resulted in complete ablation of tumor tissues with no recurrence of tumorigenesis. The antitumor photoablation effect was confirmed by ELISA for caspase-3 activity, histological analysis, and immunohistochemical TUNEL assay. In combination with drug loading to NGO in NGO−HA by $\pi-\pi$ stacking, this system can be applied for transdermal chemo- and photothermal combination therapy of melanoma skin cancers.

MATERIALS AND METHODS

Materials. Sodium salt of hyaluronic acid (HA) with a molecular weight (MW) of 100 kDa was purchased from Lifecore Co. (Chaska, MN). Hexamethylenediamine (HMDA) and chloroacetic acid were obtained from Sigma-Aldrich (St. Louis, MO). 1-Ethyl-3-(3-dimethylaminopropyl)carbodiimide (EDC) hydrochloride was purchased from Tokyo Chemical Industry Co. (Tokyo, Japan). B16F1 murine melanoma was obtained from Korean Cell Line Bank (Seoul, Korea). Detroit 551 human fetal skin fibroblast was purchased from ATCC (Manassas, VA). Dulbecco's modified Eagle's medium (DMEM), 4-(2-hydroxyethyl)-1-piperazineethanesulfonic acid (HEPES), fetal bovine serum (FBS), antibiotics, phosphate buffered saline (PBS) tablet, and 1 mM solution of Lysotracker Green DND-26 were purchased from Invitrogen Co. (Carlsbad, CA). MTT assay kit and DeadEnd Fluorometric TUNEL system were obtained from Promega Co. (Madison, WI). The 8-well glass culture slides with polystyrene vessels were purchased from BD Falcon (Franklin Lakes, NJ). Optimal cutting temperature (OCT) compound was obtained from Sakura Finetek (Zoeterwoude, The Netherlands), and Vectashield mounting medium was purchased from Vector Laboratories (Burlingame, CA). Hilyte647 Fluor 647 amine was purchased from AnaSpec (San Jose, CA), and Lissamine rhodamine B sulfonyl chloride was obtained from Life Technology (Carlsbad, CA). Caspase-3 ELISA kit was obtained from R&D System (Minneapolis, MN). Diaminobenzidine (DAB) and methyl green solution were obtained from Dako (Carpinteria, CA). All reagents were used without further purification.

Preparation of NGO−HA. Microsized GO solution was tip-sonicated and activated with chloroacetic acid in a strong basic condition to prepare carboxylated NGO (NGO−COOH). HMDA−HA was synthesized as reported elsewhere[22] and dissolved in NGO−COOH solution at a concentration of 2 mg/mL. After sonication for 5 min, NGO−HA conjugate was synthesized for 24 h by amide bond formation between a carboxyl group of NGO−COOH and an amine group of HMDA−HA using the EDC (1 mg/mL, pH 5) chemistry. After that, NGO−HA solution was dialyzed (MWCO = 3500) against DI water for 48 h. To remove free HA, NGO−HA was filtered by centrifugal filtration (MWCO = 300 kDa) at 10 000 rpm for 20 min. The control of NGO−PEG was synthesized as we reported elsewhere.[29]

***In Vitro* Photothermal Ablation Test.** B16F1 and Detroit 551 cells at a density of 6×10^3 were seeded on 96-well plates. NGO−HA was dissolved in each cell media at a concentration of 250 μg/mL and incubated for 1 h. A portable NIR laser (808 nm, Jet Lasers Photonics, Shenzhen, China) with a power density of 2 W/cm^2 was irradiated on each well for 10 min. Then, cell media were exchanged with fresh media, and the cells were incubated in 5% CO_2 incubator for 24 h. The standard MTT assay was carried out to compare the relative cell viability between cancer cells and normal fibroblast cells.

Confocal Microscopy *in Vitro* and *in Vivo*. B16F1 and Detroit 551 cells at a density of 1×10^4 were cultured on 8-well chamber plates. Hilyte647-labeled NGO−HA was incubated with both cells at 37 °C and 5% CO_2 atmosphere for 1 h. To test HA-receptor-mediated endocytosis of NGO−HA, the competitive binding test was carried out in the presence of free HA molecules. After washing with PBS three times, cells were fixed in 4% paraformaldehyde solution at room temperature for 20 min. Then, cells were mounted with Vectashield mounting medium containing 4′,6′-diamidino-2-phenylindole (DAPI). Fluorescence images were obtained under the following conditions: a pinhole size of 200 μm, the filter wavelength of 649−703 nm, and the excitation and emission wavelengths of 649 and 674 nm for Hilyte647, respectively. Furthermore, confocal laser scanning microscopy was carried out to visualize the transdermal delivery of NGO−HA−Hilyte647 to SKH-1 hairless mice with and without inoculation of B16F1 melanoma (1×10^7 cells) on the back of the mice. Hilyte647, NGO−PEG−Lissamine, or NGO−HA−Hilyte647 dissolved in DI water (1 mg/mL, 100 μL) was applied to spread on the entire skin tumor region. The administered Hilyte647, NGO−PEG−Lissamine, or NGO−HA−Hilyte647 solution was left for 30 min. Then, the skin tumor region was washed with fresh DI water three times. Each tissue was dissected, embedded in OCT compound, and sliced at a thickness of 20 μm for confocal microscopy with Leica CM 1850 cryostat (Leica, Deerfield, IL). NGO−PEG−Lissamine was visualized at the filter wavelength of 560−651 nm.

***Ex Vivo* Imaging of Dissected Tumors.** After treatment as described above, tumor tissues were dissected with skin tissue removal for *ex vivo* bioimaging of delivered NGO−HA−Hilyte647. *Ex vivo* images using IVIS imaging systems were obtained at the excitation and emission wavelength of 630 and 680 nm, respectively.

***In Vivo* Photothermal Ablation Therapy of Skin Cancer.** B16F1 cells at a density of 1×10^7 were inoculated in the dorsal flank of SKH-1 hairless mice. After a week, the tumor volume increased to an average size of 67 mm^3. Then, PBS, NGO, or NGO−HA was topically administered on the skin of the tumor for 30 min and washed with fresh DI water three times. After treatment with and without NIR irradiation, each tumor tissue was excised and fixed in 4% formaldehyde solution for 24 h. *In vivo* tests were carried out twice using three mice in each group. We have complied with the POSTECH institutional ethical protocols for animals.

Tumor Growth Monitoring. After tumor volume reached an average size of 67 mm^3, tumor growth (volume change) was monitored using the following equation: tumor volume = $A \times B^2/2$, where A and B are the maximum and minimum diameter of the tumor.[30] The relative tumor volume was calculated dividing tumor volume by initial tumor volume. Photoimage of completely photoablated tumor in mice was taken with a digital camera (Samsung, Seoul, Korea) 48 h post-treatment.

Histological Analysis of Tumor Apoptosis. Histological analysis of paraffin-embedded tumor tissue blocks with TUNEL assay was performed using DeadEnd Fluorometric TUNEL system after staining according to the manufacturer's instruction. Caspase-3 activity in excised and homogenized tumor tissues was measured with a quantitative ELISA kit according to the manufacturer's instruction. TUNEL assay for the entire tissue was carried out using anti-digoxigenin peroxidase-conjugated antibody pretreatment following DAB and methyl green staining as reported elsewhere.[31]

Conflict of Interest: The authors declare no competing financial interest.

Acknowledgment. This work was financially supported by the Converging Research Center Program through the National Research Foundation of Korea (NRF) funded by the Ministry of Education, Science and Technology (2009-0081871). This study was also supported by Midcareer Researcher Program through NRF grant funded by the MEST (No. 2012R1A2A2A06045773). We would like to thank In Tec Song and Prof. Hee Cheul Choi for the Raman spectroscopic analysis.

Supporting Information Available: Detailed materials and methods and supporting figures. This material is available free of charge *via* the Internet at http://pubs.acs.org.

REFERENCES AND NOTES

1. Dikin, D. A.; Stankovich, S.; Zimney, E. J.; Piner, R. D.; Dommett, G. H. B.; Evmenenko, G.; Nguyen, S. T.; Ruoff, R. S. Preparation and Characterization of Graphene Oxide Paper. *Nature* **2007**, *448*, 457–460.
2. Loh, K. P.; Bao, Q.; Eda, G.; Chhowalla, M. Graphene Oxide as a Chemically Tunable Platform for Optical Applications. *Nat. Chem.* **2010**, *2*, 1015–1024.
3. Markovic, Z. M.; Harhaji-Trajkovic, L. M.; Todorovic-Markovic, B. M.; Kepić, D. P.; Arsikin, K. M.; Jovanović, S. P.; Pantovic, A. C.; Dramićanina, M. D.; Trajkovic, V. S. *In Vitro* Comparison of the Photothermal Anticancer Activity of Graphene Nanoparticles and Carbon Nanotubes. *Biomaterials* **2011**, *32*, 1121–1129.
4. Robinson, J. T.; Tabakman, S. M.; Liang, Y.; Wang, H.; Casalongue, H. S.; Vinh, D.; Dai, D. Ultrasmall Reduced Graphene Oxide with High Near-Infrared Absorbance for Photothermal Therapy. *J. Am. Chem. Soc.* **2011**, *133*, 6825–6831.
5. Tian, B.; Wang, C.; Zhang, S.; Feng, L.; Liu, Z. Photothermally Enhanced Photodynamic Therapy Delivered by Nano-Graphene Oxide. *ACS Nano* **2011**, *5*, 7000–7009.
6. Bianco, A. Graphene: Safe or Toxic? The Two Faces of the Medal. *Angew.Chem., Int. Ed.* **2013**, *52*, 4986–4997.
7. Yang, K.; Zhang, S.; Zhang, G.; Sun, X.; Lee, S. T.; Liu, Z. Graphene in Mice: Ultrahigh *In Vivo* Tumor Uptake and Efficient Photothermal Therapy. *Nano Lett.* **2010**, *10*, 3318–3323.
8. Yang, K.; Wan, J.; Zhang, S.; Zhang, Y.; Lee, S. T.; Liu, Z. *In Vivo* Pharmacokinetics, Long-Term Biodistribution, and Toxicology of PEGylated Graphene in Mice. *ACS Nano* **2010**, *5*, 516–522.
9. Oh, E. J.; Choi, J. S.; Kim, H. M.; Joo, C. K.; Hahn, S. K. Anti Flt1 Peptide-Hyaluronate Conjugate for the Treatment of Retinal Neovascularization and Diabetic Retinopathy. *Biomaterials* **2011**, *32*, 3115–3123.
10. Yang, J. A.; Park, K. T.; Jung, H. T.; Kim, H. M.; Hong, S. W.; Yoon, S. K.; Hahn, S. K. Target Specific Hyaluronic Acid–Interferon Alpha Conjugate for the Treatment of Hepatitis C Virus Infection. *Biomaterials* **2011**, *32*, 8722–8729.
11. Park, J. K.; Shim, J. H.; Kang, K. S.; Yoem, J. S.; Jung, H. S.; Kim, Y. J.; Lee, K. H.; Kim, T. H.; Kim, S. Y.; Cho, D. W.; *et al.* Solid Free-Form Fabrication of Tissue-Engineering Scaffolds with a Poly(lactic-*co*-glycolic acid) Grafted Hyaluronic Acid Conjugate Encapsulating an Intact Bone Morphogenetic Protein–2/Poly(ethylene glycol) Complex. *Adv. Funct. Mater.* **2011**, *21*, 2906–2912.
12. Yang, J. A.; Kim, E. S.; Kwon, J. H.; Kim, H. M.; Shim, J. H.; Yun, S. H.; Choi, K. Y.; Hahn, S. K. Transdermal Delivery of Hyaluronic Acid–Human Growth Hormone Conjugate. *Biomaterials* **2012**, *33*, 5947–5954.
13. Brown, M. B.; Jones, S. A. Hyaluronic Acid: A Unique Topical Vehicle for the Localized Delivery of Drugs to the Skin. *J. Eur. Acad. Dermatol. Venereol.* **2005**, *19*, 308–318.
14. Banerji, S.; Wright, A. J.; Noble, M.; Mahoney, D. J.; Campbell, I. D.; Day, A. J.; Jackson, D. G. Structures of the Cd44-Hyaluronan Complex Provide Insight into a Fundamental Carbohydrate–Protein Interaction. *Nat. Struct. Mol. Biol.* **2007**, *14*, 234–239.
15. Aruffo, A.; Stamenkovic, I.; Melnick, M.; Underhill, C.; Seed, B. CD44 Is the Principal Cell Surface Receptor for Hyaluronate. *Cell* **1990**, *61*, 1303–1313.
16. Schledzewski, K.; Falkowski, M.; Moldenhauer, G.; Metharom, P.; Kzhyshkowska, J.; Ganss, R.; Demory, A.; Falkowska-Hansen, B.; Kurzen, H.; Ugurel, S.; *et al.* Lymphatic Endothelium-Specific Hyaluronan Receptor LYVE-1 Is Expressed by Stabilin-1+, F4/80+, CD11b+ Macrophages in Malignant Tumours and Wound Healing Tissue *in Vivo* and in Bone Marrow Cultures *in Vitro*: Implications for the Assessment of Lymphangiogenesis. *J. Pathol.* **2006**, *209*, 56–66.
17. Creixell, M.; Bohórquez, A. C.; Lugo, M. T.; Rinaldi, C. EGFR-Targeted Magnetic Nanoparticle Heaters Kill Cancer Cells without a Perceptible Temperature Rise. *ACS Nano* **2011**, *5*, 7124–7129.
18. Huang, X.; Jain, P. K.; El-Sayed, I. H.; El-Sayed, M. A. Determination of the Minimum Temperature Required for Selective Photothermal Destruction of Cancer Cells with the Use of Immunotargeted Gold Nanoparticles. *Photochem. Photobiol.* **2006**, *82*, 412–417.
19. Fortin, J. P.; Wilhelm, C.; Servais, J.; Ménager, C.; Bacri, J. C.; Gazeau, F. Size-Sorted Anionic Iron Oxide Nanomagnets as Colloidal Mediators for Magnetic Hyperthermia. *J. Am. Chem. Soc.* **2007**, *129*, 2628–2635.
20. Moon, M. K.; Lee, S. H.; Choi, H. C. *In Vivo* Near-Infrared Mediated Tumor Destruction by Photothermal Effect of Carbon Nanotubes. *ACS Nano* **2009**, *3*, 3707–3713.
21. Rhodes, A. R. Public Education and Cancer of the Skin. What Do People Need To Know about Melanoma and Nonmelanoma Skin Cancer? *Cancer* **1995**, *75*, 613–636.
22. Yoem, J. S.; Bhang, S. H.; Kim, B. S.; Seo, M. S.; Hwang, E. J.; Cho, I. H.; Park, J. K.; Hahn, S. K. Effect of Cross-Linking Reagents for Hyaluronic Acid Hydrogel Dermal Fillers on Tissue Augmentation and Regeneration. *Bioconjugate Chem.* **2010**, *21*, 240–247.
23. Zhou, W.; Shao, J.; Jun, Q.; Wei, Q.; Tang, J.; Ji, J. Zwitterionic Phosphorylcholine as a Better Ligand for Gold Nanorods Cell Uptake and Selective Photothermal Ablation of Cancer Cells. *Chem. Commun.* **2010**, *46*, 1479–1481.
24. Elengoe, A.; Hamdan, S. Heat Sensitivity between Human Normal Liver (WRL-68) and Breast Cancer (MCF-7) Cell Lines. *J. Biotechnol. Lett.* **2013**, *4*, 45–50.
25. Rudrabhatla, S. R.; Mahaffey, C. L.; Mummert, M. E. Tumor Microenvironment Modulates Hyaluronan Expression: The Lactate Effect. *J. Invest. Dermatol.* **2006**, *126*, 1378–1387.
26. Yoshida, H.; Nagaoka, A.; Kikushima, A. J.; Tobiishi, M.; Kawabata, K.; Sayo, T.; Sakai, S.; Sugiyama, Y.; Enomoto, E.; Okada, Y.; *et al.* KIAA1199, a Deafness Gene of Unknown Function, Is a New Hyaluronan Binding Protein Involved in Hyaluronan Depolymerization. *Proc. Natl. Acad. Sci. U.S.A.* **2013**, *110*, 5612–5617.
27. Lopez, R. F. V.; Lange, N.; Guy, R.; Bentley, M. V. L. B. Photodynamic Therapy of Skin Cancer: Controlled Drug Delivery of 5-ALA and Its Esters. *Adv. Drug Delivery Rev.* **2004**, *56*, 77–94.

28. Heijn, M.; Roberge, S.; Jain, R. K. Cellular Membrane Permeability of Anthracyclines Does Not Correlate with Their Delivery in a Tissue Isolated Tumor. *Cancer Res.* **1999**, *59*, 4458–4463.
29. Kong, W. H.; Sung, D. K.; Kim, K. S.; Jung, H. S.; Gho, E. J.; Yun, S. H.; Hahn, S. K. Self-Assembled Complex of Probe Peptide–*E. coli* RNA I Conjugate and Nano Graphene Oxide for Apoptosis Diagnosis. *Biomaterials* **2012**, *33*, 7556–7564.
30. Hoeck, J. D.; Jandke, A.; Blake, S. M.; Nye, E.; Dene, B. S.; Brandner, S.; Behrens, A. Fbw7 Controls Neural Stem Cell Differentiation and Progenitor Apoptosis *via* Notch and c-Jun. *Nat. Neurosci.* **2010**, *13*, 1365–1372.
31. Yao, Y. M.; Liu, Q. G.; Yang, W.; Zhang, M.; Ma, Q. Y.; Pan, C. E. Effect of Spleen on Immune Function of Rats with Liver Cancer Complicated by Liver Cirrhosis. *Hepatobiliary Pancreatic Dis. Int.* **2003**, *2*, 242–246.